JACS
JOURNAL OF THE AMERICAN CHEMICAL SOCIETY
pubs.acs.org/JACS
Article

Kinetic, Thermodynamic, and Dynamic Control in Normal vs. Cross [2 + 2] Cycloadditions of Ene-Keteniminium Ions: Computational Understanding, Prediction, and Experimental Verification

Pan Zhang and Zhi-Xiang Yu*

Cite This: J. Am. Chem. Soc. 2023, 145, 9634–9645
Read Online

ABSTRACT: Almost all reported intramolecular [2 + 2] reactions of ene-keteniminium ions gave normal [2 + 2] products with a fused bicycle framework, but not cross [2 + 2] products with a bicyclo[3.1.1]heptane skeleton, a highly pursued bioisostere in pharmaceutical chemistry. How to rationalize this and design new cross [2 + 2] reactions? Theoretical studies using density functional theory, high-level *ab initio* single-point energy calculations, and molecular dynamics showed that this [2 + 2] reaction has all three patterns of regiochemical control: the reaction is controlled either kinetically, thermodynamically, or dynamically. A carbocation model of forming *endo* and *exo* carbocations has been proposed to rationalize the reaction outcomes, revealing that the tethers (between alkenes and keteniminium ions), substituents (on the alkenes), and alkene configurations in ene-keteniminium ions play critical roles. These understandings were further used to predict that introducing a substituent in the terminal position of alkene with a *trans* configuration in ene-keteniminium ions can realize the cross [2 + 2] reaction, which is dynamically controlled for alkyl substituents or kinetically controlled for aryl substituents. These and more other predictions were realized experimentally, and many cross [2 + 2] products with a bicyclo[3.1.1]heptane skeleton can be achieved. Both molecular dynamics and new experiments have also been applied to correct a key but misassigned [2 + 2] product reported in the literature, further supporting the insightful mechanisms reported here.

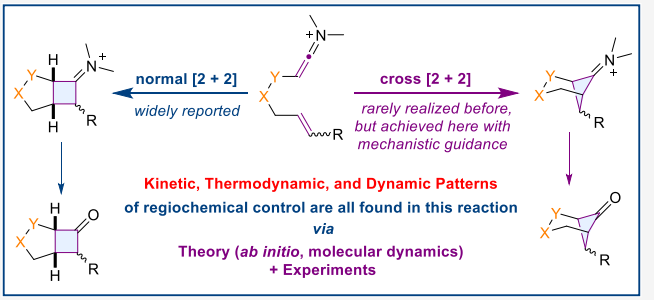

INTRODUCTION

Bicyclic cyclobutanones, which are important and synthetically challenging molecules and intermediates in organic synthesis, can be synthesized by intramolecular [2 + 2] cycloadditions of ketenes with alkenes.[1] The intramolecular [2 + 2] cycloadditions can give either normal or cross [2 + 2] cycloadducts (Scheme 1). Previously, we have studied the mechanism of the [2 + 2] cycloaddition of ene-ketenes,[2,3] finding that this reaction is kinetically controlled and the relative stabilities of the generated (formal) carbocations, labeled as *endo* (or internal) and *exo* (or external) carbocations in the corresponding concerted [2 + 2] transition states, determine the regiochemistry.

In some cases, the reactivities of used ketenes are poor; chemists (pioneered by Ghosez and Snider) then applied the intramolecular [2 + 2] reactions of ene-keteniminium ions,[1a−d,4,5] which are equivalents of [2 + 2] reactions of ene-ketenes, considering that hydrolysis of the cycloadducts from ene-keteniminium ions gave the same products, namely, cyclobutanones. Interestingly, almost all reported intramolecular [2 + 2] reactions of ene-keteniminium ions gave normal [2 + 2] cycloadducts, as can be appreciated from selected examples in Scheme 2. Only in a few cases were both normal and cross [2 + 2] products observed. We tried to understand the mechanism of this [2 + 2] reaction and the factors affecting its regiochemistry, which is our primary goal in this study. We were also interested in using the mechanistic insights to realize experimentally the cross [2 + 2] reaction of ene-keteniminium ions so that we can provide a new way to synthesize molecules with a challenging bicyclo[3.1.1]heptane skeleton, which is important in the synthesis and is also a highly pursued bioisostere in medicinal chemistry.[6]

In the beginning, we tried to just apply our previous model of carbocations in the [2 + 2] reaction of ene-ketenes to understand the regiochemistry of ene-keteniminium ions and guide us in designing and realizing cross [2 + 2] cycloadditions. Unfortunately, such attempts encountered failure. For example, **1F** gave only a normal product, while **1G** gave both normal and cross [2 + 2] products, although the difference between these two substrates is just the different tethers between keteniminium ions and alkenes in the

Received: January 18, 2023
Published: April 19, 2023

https://doi.org/10.1021/jacs.3c00685
J. Am. Chem. Soc. 2023, 145, 9634–9645

Scheme 1. Intramolecular [2 + 2] Cycloadditions of Ene-Ketenes and Ene-Keteniminium Ions

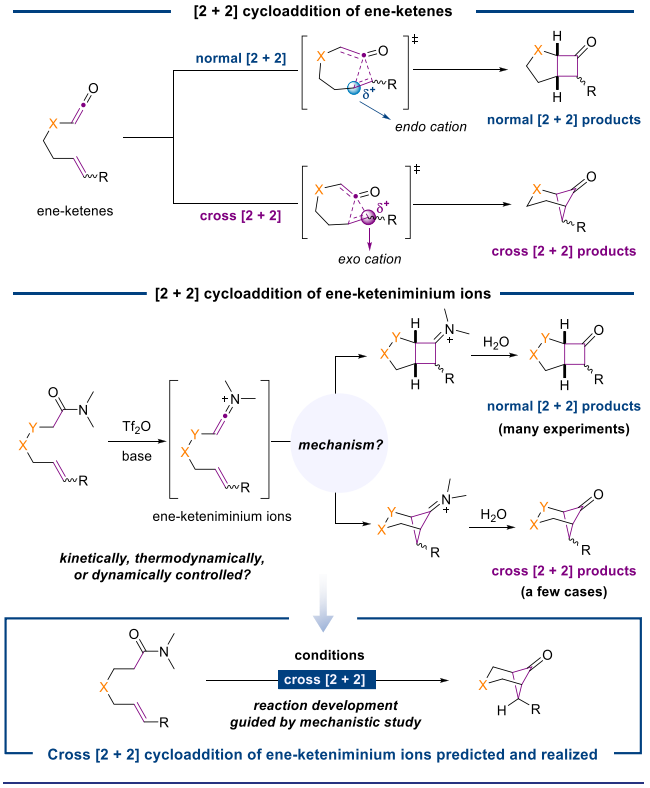

substrates (Scheme 2). Therefore, detailed mechanistic studies of different reactions reported in the literature should be scrutinized by *ab initio* calculations.

We point out that during our preparation of this manuscript, Maulide and Houk reported their insightful mechanism of the [2 + 2] reaction of ene-keteniminium ions, which was found to be kinetically controlled for their substrates.[7,8] In our study reported here, the intramolecular [2 + 2] reactions of ene-keteniminiums, with more examples compared to those in Maulide and Houk's paper, are very complex. We found that the regiochemistry[9] in some cases is kinetically controlled. But in other cases, the reaction is thermodynamically controlled. To our surprise, some [2 + 2] reactions are dynamically controlled.[9−11] The existence of all three regiochemical control patterns (kinetic, thermodynamic, and dynamic controls of regiochemistry) is unprecedented, to the best of our knowledge. We report here all these findings, together with a carbocation model to rationalize the whole mechanistic spectrum of [2 + 2] reactions of ene-keteniminium ions. Furthermore, to our excitement, we used this model and mechanistic understanding to correct a key experimental result reported in the literature. This mechanistic model was also applied to guide us to realize the rarely observed cross [2 + 2] reactions of ene-keteniminium ions. These predictions and experimental verification are also reported here.

RESULTS AND DISCUSSION

We found that the mechanistic scenario of [2 + 2] cycloaddition of ene-keteniminium ions with α-O tethers is different from that of ene-keteniminium ions with β-N tethers. Thus, we discuss these two scenarios separately.

Intramolecular [2 + 2] Cycloadditions of Ene-Keteniminium Ions with α-O Tethers. We calculated the Gibbs energy profiles of [2 + 2] cycloadditions of different ene-keteniminium ions with different substitution patterns on their alkene moiety. The Gibbs energy profile of **1a** is shown in Figure 1a. This ene-keteniminium ion can undergo cyclopropanation to generate the 6/3 fused bicyclic intermediate **IN-1a** with an activation free energy of 10.3 kcal/mol via **TS1-1a**. This process is exergonic by 11.5 kcal/mol. Subsequently, **IN-1a** can undergo rearrangement to give both the normal [2 + 2] product (NP) **NP-1a** and cross [2 + 2] product (CP) **CP-1a** via **TS2-1a** and **TS3-1a**, respectively. The normal pathway via **TS2-1a**, which resembles an *endo* tertiary carbocation, is 6.1 kcal/mol more favored compared to the cross pathway via **TS3-1a**, which resembles an *exo* primary carbocation. Thus, this reaction is kinetically controlled and only the normal [2 + 2] product could be observed, which is consistent with the experiment[1d] (Scheme 2, reaction 1). We also found that **1b** (the keteniminium ion formed by **1B**) shares a similar Gibbs energy profile, which is given in the Supporting Information (SI).

The reaction outcomes were different for the substrates with a substitution in the terminal position of the alkene. The Gibbs energy profiles for **1c** with a methyl substitution are shown in Figure 1b. For *Z*-type ene-keteniminium ion **1c**, cyclopropanation occurs first via **TS1-1c** with an activation free energy of 12.2 kcal/mol to form a 6/3 fused bicycle intermediate **IN-1c**. However, the cross [2 + 2] pathway via **TS3-1c** leading to **CP-1c** becomes more favored (3.5 kcal/mol lower than the normal [2 + 2] cycloaddition via **TS2-1c** leading to **NP-1c**). Here, the cross [2 + 2] pathway is favored, requiring less conformation change from **IN-1c** to **TS3-1c** compared to that in the normal [2 + 2] pathway. This is consistent with experimental observations that **3C** was the major product when the reaction time was short (Scheme 2, reaction 3). But **CP-1c** is not stable compared to **NP-1c**, and it can isomerize to **NP-1c** under the reaction conditions, considering that the activation free energy for this isomerization is 30.9 kcal/mol, which can be achieved for the reaction at 85 °C. Therefore, the ratio of **NP-1c**:**CP-1c** became larger when the reaction time increased.[1d] This computational rationalization is consistent with the experimental observation that longer reaction times gave more normal [2 + 2] products (Scheme 2, reaction 3).

The Gibbs energy profile of *E*-type ene-keteniminium ion **1d** is similar to that of **1c** (see the SI for details). The only difference is that the cyclopropane intermediate could undergo proton transfer to give **FC** (similar to an ene reaction), which can then be hydrolyzed to give the Friedel−Crafts product (Figure 1d).[1d] Although the cross [2 + 2] product is kinetically favored, the Friedel−Crafts product is thermodynamically more stable and becomes the observed product. It should be noted that only ene-keteniminium ions with an *E*-alkene could go through the Friedel−Crafts pathway since the proton transfer process requires that the alkyl group and NMe_2 are in a *cis* configuration.

Thus, as shown in Figure 1c, we can conclude that the reaction selectivity is controlled kinetically for α-*O*-tethered ene-keteniminium ions with internal alkyl-substituted alkenes or terminal alkenes. The normal [2 + 2] pathway is more favored because its rearrangement transition state with tertiary or second carbocation character is more stable than the transition state with primary carbocation character in the cross [2 + 2] pathway. For α-*O*-tethered ene-keteniminium ions with external alkyl-substituted alkenes, the reaction selectivity is

https://doi.org/10.1021/jacs.3c00685
J. Am. Chem. Soc. 2023, 145, 9634−9645

Scheme 2. Experimental Reaction Outcomes of [2 + 2] Cycloadditions of Different Ene-Keteniminium Ions[a]

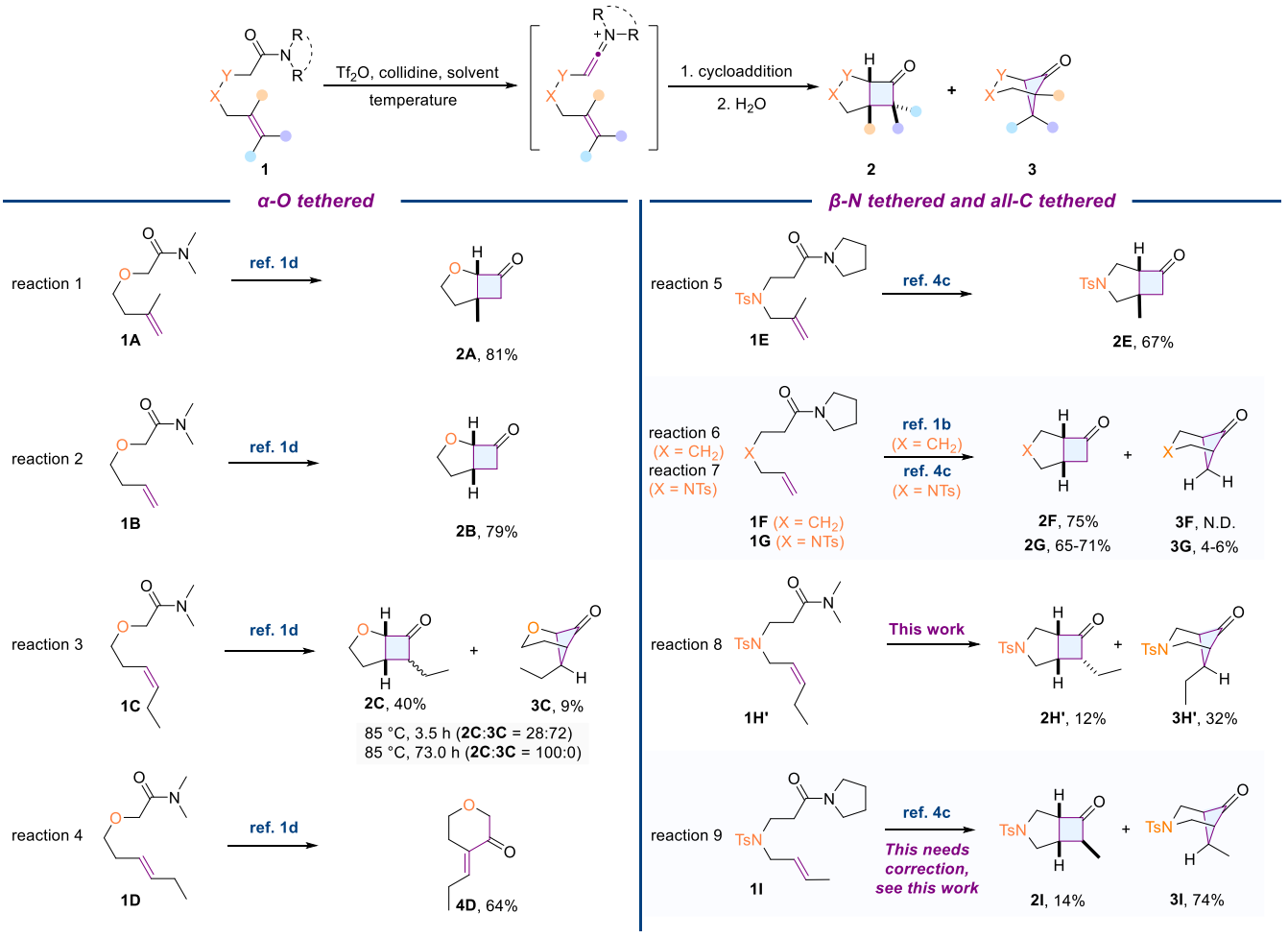

[a]The detailed reaction conditions can be found in the corresponding references. N.D., not detected.

thermodynamically controlled because the kinetically more favored cross [2 + 2] product could isomerize to a more stable normal [2 + 2] or Friedel−Crafts product (Figure 1d).

Intramolecular [2 + 2] Cycloadditions of Ene-Keteniminium Ions with *β*-N Tether: Theory and Experiments. To know the origins responsible for the mechanistic differences, we explored the reaction pathways of different *β*-N-tethered ene-keteniminium ions computationally and experimentally. After delivering these results, we will then present a general model to explain the reaction selectivity.

For **1e**, a concerted asynchronous [2 + 2] cycloaddition process, giving the normal cycloadduct **NP-1e** via **TS1-1e**, was found (Figure 2). Relaxed potential energy surface (PES) scan indicated that there are no post-transition state bifurcation[9−11] characteristics (see the SI for details). The normal [2 + 2] reaction has an activation free energy of 12.5 kcal/mol. Different from **1a**, the [2 + 2] cycloaddition process is concerted and no 6/3 bicyclic intermediate like **IN-1a** could be generated because there is no *α-O* that can stabilize the cyclopropyl cation. Isomerization from **NP-1e** to **CP-1e** is almost impossible under reported reaction conditions because this requires an activation free energy of about 50 kcal/mol.[12] This is consistent with previous experiments (Scheme 2, reaction 5).

But we found that the control pattern of regiochemistry of [2 + 2] of ene-keteniminium ions changes to a dynamically controlled one for substrate **1h**, which has an internal alkene with *Z* configuration. Calculations indicated that both **IN1-1h** and **CP-1h** are connected by the [2 + 2] cycloaddition transition state **TS1-1h** (Figure 3a). Isomerization of **IN1-1h** gives **NP-1h**, almost without a barrier. The activation free energy of interconversion (40.1 kcal/mol from **CP-1h** to **TS3-1h**) is very high, suggesting that the regiochemistry for **1h** is controlled dynamically, not thermodynamically. We then performed quasi-classical trajectory (QCT) molecular dynamics simulations to predict the distribution of normal and cross [2 + 2] products for **1h** (Figure 3b), finding that the ratio of NP/CP is 1:3.5 (30 NP, 104 CP, and 9 recrossing to form again the starting materials). To validate the theoretical prediction, we then synthesized an analogue of **1h**, which is **1H′** with an ethyl instead of a methyl group in its alkene moiety. The [2 + 2] cycloaddition of **1H′** produced **3H′** and **2H′** with reaction yields of 32 and 12% (Figure 3a), respectively, which nicely supported our molecular dynamics simulations.

To obtain more information about the origin of post-transition state bifurcation, we analyzed the normal and cross trajectories of [2 + 2] cycloaddition of **1h** in detail (Figure 3). In the normal [2 + 2] cycloaddition, two different kinds of

https://doi.org/10.1021/jacs.3c00685
J. Am. Chem. Soc. 2023, 145, 9634−9645

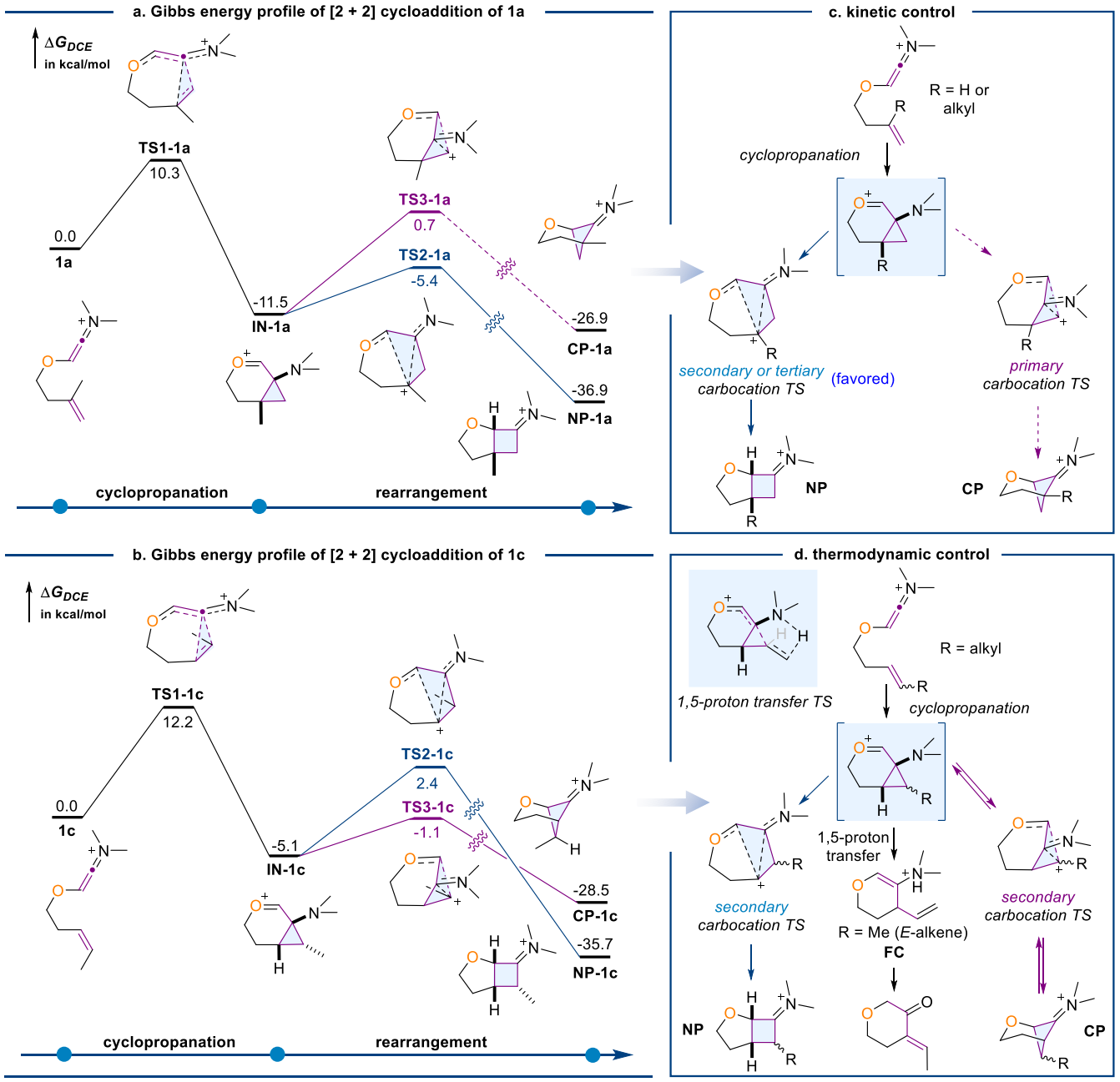

Figure 1. (a–d) Mechanisms for [2 + 2] cycloadditions of *α*-*O*-tethered ene-keteniminium ions. Computed at the DLPNO-CCSD(T)/cc-pVTZ:SMD(DCE)//*ω*B97X-D/def2-SVP level.

trajectories can be found. The first type of trajectory passed through a short-lived *endo* carbocation, **IN1-1h** (Figure 3c). Another type of trajectory passed through a long-lived *endo* carbocation (Figure 3d), which means that the reaction passes through a zone forming the C6–C7 bond, while the C4–C5 bond formation delays for a long lifetime. Most trajectories leading to the normal [2 + 2] products passed through long-lived *endo* carbocations, which means that the time gap between forming the first bond and the second bond is longer than 300 fs[13] (see the SI). A similar phenomenon can be also observed in the two representative cross [2 + 2] trajectories (Figure 3e,f). Meanwhile, only about a half of trajectories leading to the cross [2 + 2] products passed through long-lived *exo* carbocations (see the SI). The *exo* carbocation region in the cross [2 + 2] trajectories could be an entropic intermediate[13,14] according to the variational transition state theory (VTST)[15] calculations (see the SI for details). Such an entropic intermediate could be located as a real intermediate in the solution phase (see the SI). Solution phase molecular dynamics simulation (see the SI) gave a similar result (NP/CP = 1:3.4) with that in the gas phase, indicating that structure optimization and molecular dynamics simulation in the gas and solution phases did not have a dramatic difference. It should be noted that the interconversion between the *endo* carbocation and *exo* carbocation via **TS3-1h** is possible in both normal and cross [2 + 2] trajectories.

The *exo* (in cross [2 + 2] trajectories) and *endo* carbocations (in normal [2 + 2] trajectories) are both secondary carbocations and have similar stabilities. Consequently, post-transition state bifurcation would occur because the two

https://doi.org/10.1021/jacs.3c00685
J. Am. Chem. Soc. 2023, 145, 9634–9645

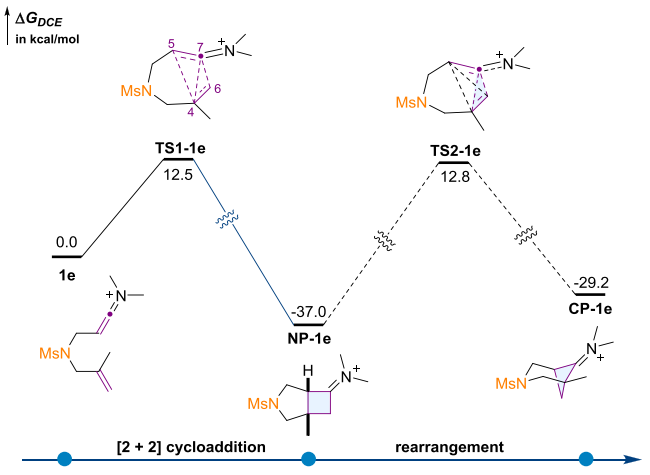

Figure 2. Gibbs energy profile of [2 + 2] cycloaddition of **1e**. Computed at the DLPNO-CCSD(T)/cc-pVTZ:SMD(DCE)//ωB97X-D/def2-SVP level.

trajectories, passing through *endo* and *exo* carbocations with similar stabilities, are both energetically feasible.

Therefore, comparing the relative stabilities of the *endo* and *exo* carbocations, which is named here as the carbocation model, can tell us the reaction outcomes (Scheme 3; here, R^1 and R^2 are H or alkyl groups). The normal [2 + 2] cycloaddition would pass through the *endo* carbocation region, while the cross [2 + 2] cycloaddition would pass through the *exo* carbocation region. Whether post-transition state bifurcation would occur is determined by the relative stability of these two types of carbocation. If the formed *endo* and *exo* carbocations in the reaction process are comparable in stability, post-transition state bifurcation would occur. This is the case for **1h**. If the *endo* carbocation is much more stable than the *exo* carbocation, the selectivity could be kinetically controlled and the normal [2 + 2] product would be favored over the cross [2 + 2] product. This is the case for **1e**. The cross [2 + 2] product would be kinetically favored over the normal [2 + 2] product if the *exo* carbocation is much more stable (see the prediction and experimental part below).

We must point out that there are many combinations of R^1, R^2, and X for the [2 + 2] reactions of ene-keteniminium ions and the carbocation model in Scheme 3 could be modified, as can be seen from later studies shown in Figure 5 with different configurations of alkene in the substrates and Figure 7a with R^1 = aryl groups.

Validation of the Carbocation Model, Correction of the Literature Report, and Realization of the Cross [2 + 2] Reaction. To further support our carbocation model, we studied the [2 + 2] cycloaddition of **1i** computationally and experimentally (Figure 4), which is different from **1h** by the geometry of the double bond. Our model predicted that the [2 + 2] reaction of substrate **1i** is also dynamically controlled. The Gibbs energy profile is given in Figure 4a. **TS-1i** is ambimodal leading to normal [2 + 2] cycloadduct **NP-1i** and cation intermediate **IN-1i**, which then affords cross [2 + 2] product **CP-1i** with a quite low barrier. Molecular dynamics simulations (Figure 4b) indicated that 189 among 206 trajectories lead to **IN-1i**, which could finally give the final cross [2 + 2] product, and only 2 trajectories lead to **NP-1i** (another 15 recross to give back the starting materials). Accordingly, the ratio of CP:NP should be about 95:1, which is in contrast to the previous experimental report (CP/NP = 5:1; see reaction 9 in Scheme 2). This discrepancy between calculations and experiments prompted us to repeat the experiment.

To our surprise, using the same substrate **1I** (Figure 4c), we did not observe the normal [2 + 2] product, but two different cross [2 + 2] products, which are stereoisomers (**3I**/**3H** = 5:1). What is more, a similar result (**3I**/**3H** = 6:1) was also obtained when we tested substrate **1I′** with a dimethylamino group (Figure 4c). This means that **3H** was mistakenly assigned as the normal [2 + 2] product **2I** in the original report.[4c]

In the original experiment, the substrate was a mixture of *E*/*Z* ene-keteniminium ions (although the authors may be not aware of it). We hypothesized that *E* substrate **1I′** (methyl analogue of **1I**) gave **3I** as the major product while the *Z* substrate mainly gave **3H**. To confirm this prediction, we then synthesized **1I′** with improved purity (*E*/*Z* = 11:1) using a new method (see the SI). To our delight, the **3I**/**3H** ratio (19:1) became much larger when this substrate was tested (Figure 4c). This result supported our molecular dynamics simulations and disproved the original report. Here, we emphasize that this new experiment can represent a new example of the cross [2 + 2] reaction of ene-keteniminium ions.

The cross [2 + 2] cycloaddition of ene-keteniminium ions has been rarely realized. With the above success of interplay of theory and experiment, we predicted that other alkyl-substituted substrates of ene-keteniminium ions would give also cross [2 + 2] products in a dynamically controlled manner. We tested several more examples experimentally, finding that two new substrates **1J** and **1K** (with *E*-alkene) gave cross [2 + 2] products exclusively (see Figure 4d).

Dimethyl-substituted **1L** (Figure 4e) was also predicted to give the cross [2 + 2] product because the generated *exo* carbocation is a tertiary carbocation, according to our carbocation model shown in Scheme 3. However, our experimental result showed that product **4L** was formed in 38% yield, not the cross [2 + 2] product. This can be explained by the fact that a competing ene reaction pathway via 1,5-proton transfer was favored over the ring formation (Figure 4e), which is also supported by calculation results (see the SI).

Understanding of How the *E*/*Z* Configurations Affect the Dynamic Outcomes? Here, we provide an understanding of why substrates with *Z* configuration of alkene have two products while substrates with *E* configuration have one product detected experimentally (Figure 5; *R* = alkyl group). For the *E* substrate, the formed *endo*-E carbocation with a seven-membered ring structure is less stable than *exo*-E carbocation with a six-membered ring structure (this is supported by calculations that optimization of the *endo*-E cation directly went to the *exo*-E cation). Consequently, this dynamically controlled reaction gave CP dominantly. This can explain experimental results that only cross [2 + 2] products were observed (Figure 4).

But for the substrate with a *Z*-alkene, the *exo*-Z cation experiences some repulsion. Consequently, both *endo* and *exo* carbocations have similar stabilities (for *X* = NMs, *R* = Me, the free energy difference in solution is 0.2 kcal/mol). Qualitatively, we can then predict that both NP and CP should be obtained.[11k] This can explain the experimental results (Figure 3a).

https://doi.org/10.1021/jacs.3c00685
J. Am. Chem. Soc. 2023, 145, 9634−9645

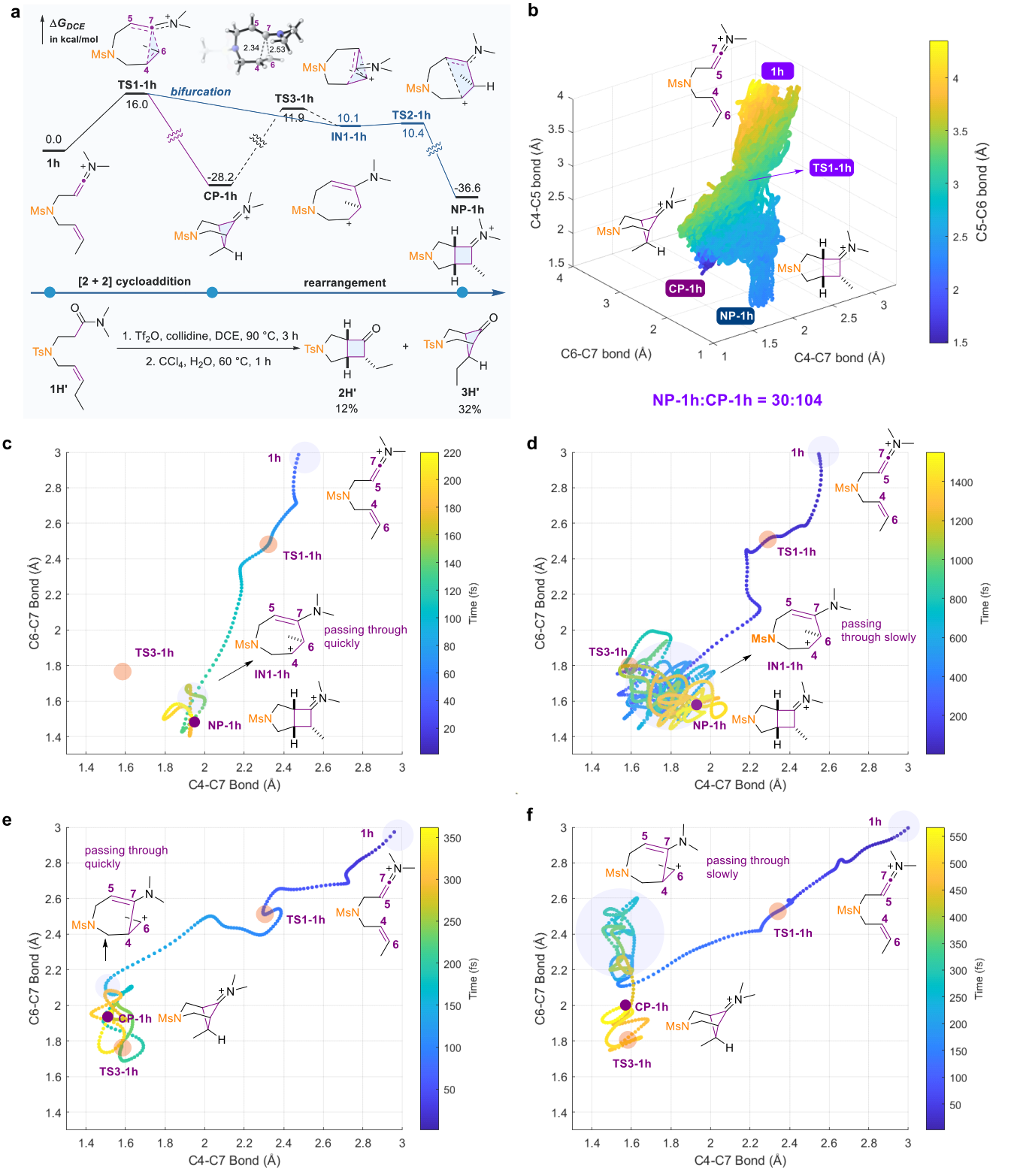

Figure 3. Gibbs energy profile, experimental validation, and QCT molecular dynamics simulations of [2 + 2] cycloaddition of **1h**. (a) Gibbs energy profile of **1h** (computed at the DLPNO-CCSD(T)/cc-pVTZ:SMD(DCE)//ωB97X-D/def2-SVP level) and experimental validation of computation results. The bond lengths are reported in Å. The yields given are average yields of isolated products for two runs. (b) QCT molecular dynamics simulations of **1h**. (c) Representative trajectory with short-lived *endo* carbocation of the normal [2 + 2] pathway for **1h**. (d) Representative trajectory with long-lived *endo* carbocation of the normal [2 + 2] pathway for **1h**. (e) Representative trajectory with short-lived *exo* carbocation of the cross [2 + 2] pathway for **1h**. (f) Representative trajectory with long-lived *exo* carbocation of the cross [2 + 2] pathway for **1h**.

Special Case: Hydrogen-Bonding and Inductive Effect Induced Bifurcation. Although the carbocation model is useful, we found it difficult to explain the reaction outcomes of **1F** and **1G** (Scheme 2), both of which should give

https://doi.org/10.1021/jacs.3c00685
J. Am. Chem. Soc. 2023, 145, 9634−9645

Scheme 3. Carbocation Model to Predict the Selectivity of [2 + 2] Cycloadditions of Ene-Keteniminium Ions[a]

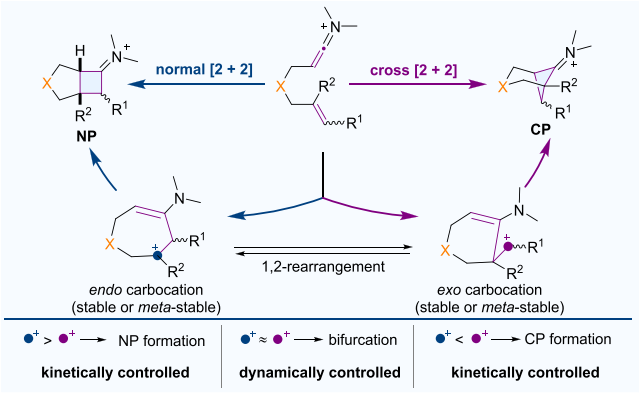

[a]>, more stable than; ≈, comparable stable as; <, less stable than (R^1 and R^2 are H or alkyl groups).

the normal [2 + 2] products, based on our carbocation model. This is because the generation of *endo*-secondary carbocation in the normal [2 + 2] reaction pathway for these two substrates is favored over the generation of primary *exo* carbocation in the cross [2 + 2] reaction (Figure 6a,b). Experimentally, **1F** only gave the normal [2 + 2] cycloaddition product, agreeing with this model, but **1G** delivered both normal and cross [2 + 2] cycloaddition products (Scheme 2).

Our calculations showed that the reaction of **1f** (the corresponding ene-keteniminium ion analogue of **1F**; see the SI for details) favors the normal [2 + 2] pathway because generation of the *endo* carbocation in this pathway is favored. Consequently, only one product was generated. But to our surprise, the reaction of **1G** is dynamically controlled (Figure 6b,c). This is because the tether in this substrate is an NTs group, which can stabilize the primary carbocation in the cross [2 + 2] pathway (a detailed analysis via noncovalent interactions (NCI) for the hydrogen-bonding interaction can

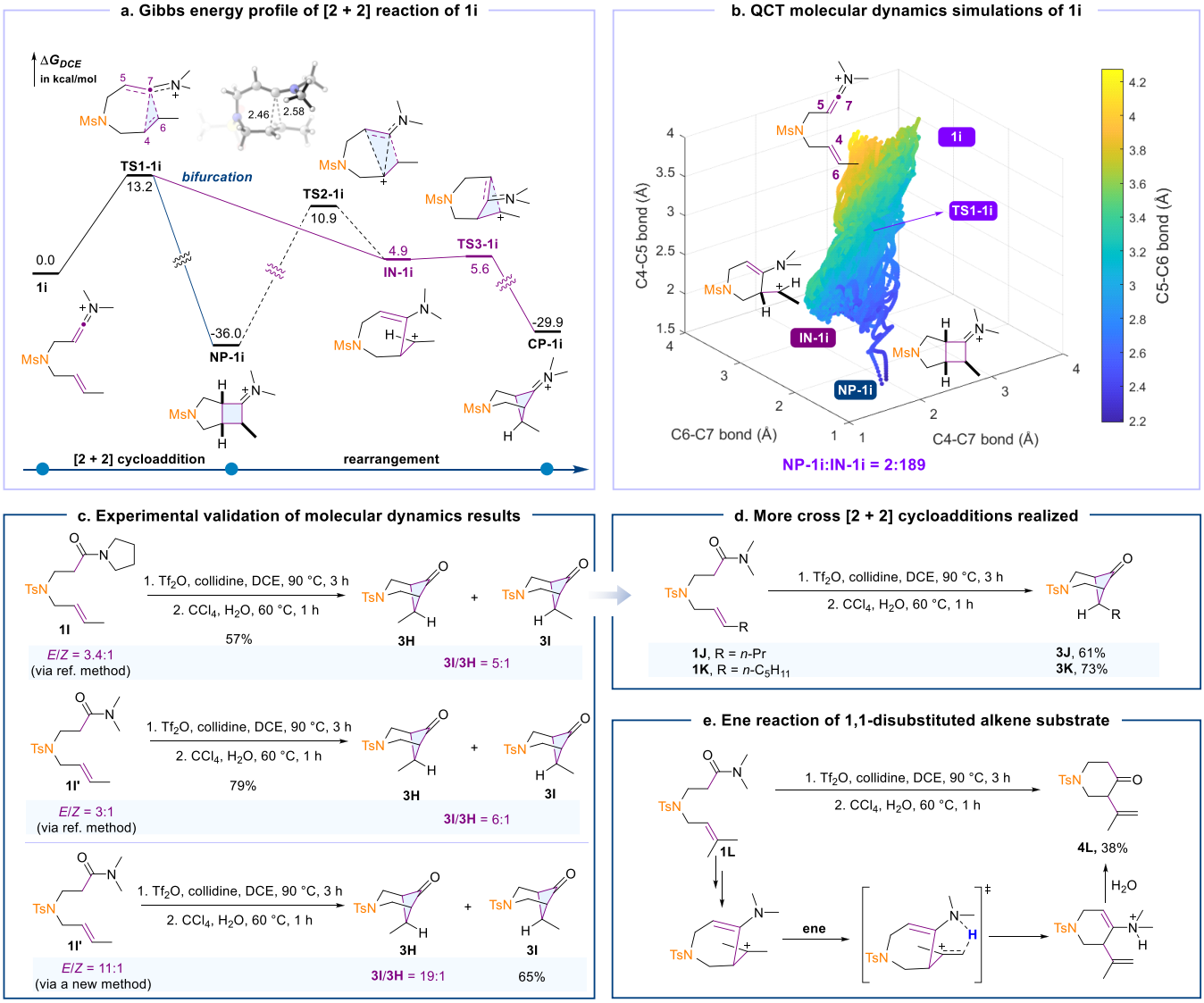

Figure 4. (a–e) Computations and new experiments to correct the literature report and realize new cross [2 + 2] cycloadditions. All the given ratios of new compounds in the experiments were determined by ^{1}H NMR. The Gibbs energy profile was computed at the DLPNO-CCSD(T)/cc-pVTZ:SMD(DCE)//ωB97X-D/def2-SVP level. The bond lengths are reported in Å. The yields given are average yields of isolated products for two runs.

https://doi.org/10.1021/jacs.3c00685
J. Am. Chem. Soc. 2023, 145, 9634–9645

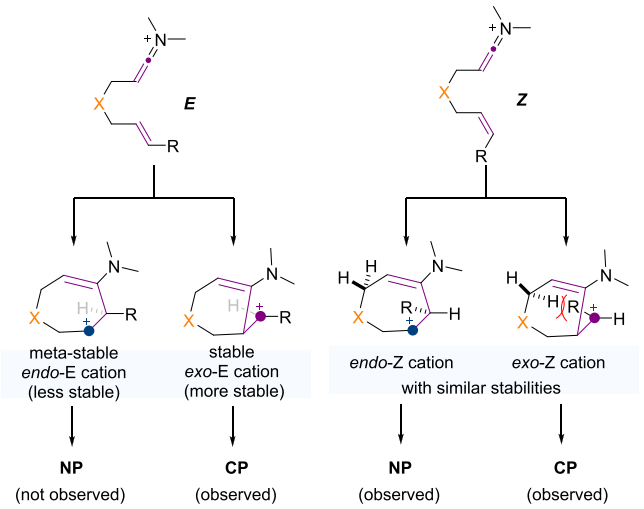

Figure 5. Carbocation model to rationalize selectivity of substrates with different alkene configurations when *R* = alkyl group.

be found in the SI). In addition, the *endo* carbocation was destabilized by the inductive effect of the NMs group of **1g**. Consequently, the primary and secondary carbocations here have similar stabilities, and the reaction then favors bifurcation.

To confirm this finding, QCT molecular dynamics simulations (Figure 6c) were performed to confirm the selectivity. Starting from **TS1-1g**, there are 175 out of 198 trajectories leading to the normal [2 + 2] cycloadduct (**NP-1g**), while 18 trajectories afforded the cross [2 + 2] cycloadduct (**CP-1g**), and 5 trajectories recrossed to give back to the starting material. These results predicted that the ratio of normal [2 + 2] product and cross [2 + 2] product should be about 10:1. This is close to the experimental result (14:1, Scheme 2, reaction 7).

However, there is no such hydrogen-bonding and inductive effect for **1f**, and no bifurcation can be observed. Thus, the reaction gives **NP-1f** in a kinetically controlled manner (Figure 6a).

Why Intramolecular [2 + 2] Reactions of Ene-Ketenes and Ene-Keteniminium Ions Have Different Mechanisms? Our previous study[2] showed that almost all the intramolecular [2 + 2] cycloadditions for ene-ketenes are kinetically controlled. But here, some [2 + 2] cycloaddition transition states of ene-keteniminium ions are ambimodal. Why? We attributed this difference to high reactivity of keteniminium ions with respect to that of ketenes.[1a,4a] Consequently, the [2 + 2] cycloaddition transition states in ene-keteniminium ions are very early and the distances of two forming bonds (C4−C7 and C6−C7) are close (e.g., see **TS1-1h** in Figure 3 and **TS1-1i** in Figure 4), which makes both *endo* and *exo* carbocations have similar stabilities and an ambimodal transition state can be realized. But for ene-ketenes, the corresponding transition states are late (the forming bond is much shorter than the other bond), much more like the products (see the SI). As a result, no bifurcation conditions can be found. The different reaction patterns of ene-ketenes and ene-keteniminium ions with α-O tethers were also discussed, which are given in the SI.

More Predictions of Cross [2 + 2] Reactions of Ene-Keteniminium Ions with Aryl Substituents and Experimental Verification. We further predicted that for substrates with an aryl group in the *E*-alkene part, the reaction would give cross [2 + 2] products in a kinetically controlled fashion because an *exo* carbocation ***E*-Ar-Cat** with the aryl substituent in this pathway is much more favored over the *endo* carbocation ***E*-Ar-Cat′**, which is not a minimum and isomerizes to *exo* carbocation in geometry optimization calculations (Figure 7a). Calculations using **1m** (an analogue keteniminium ion of **1M**; see the SI for details) as a model

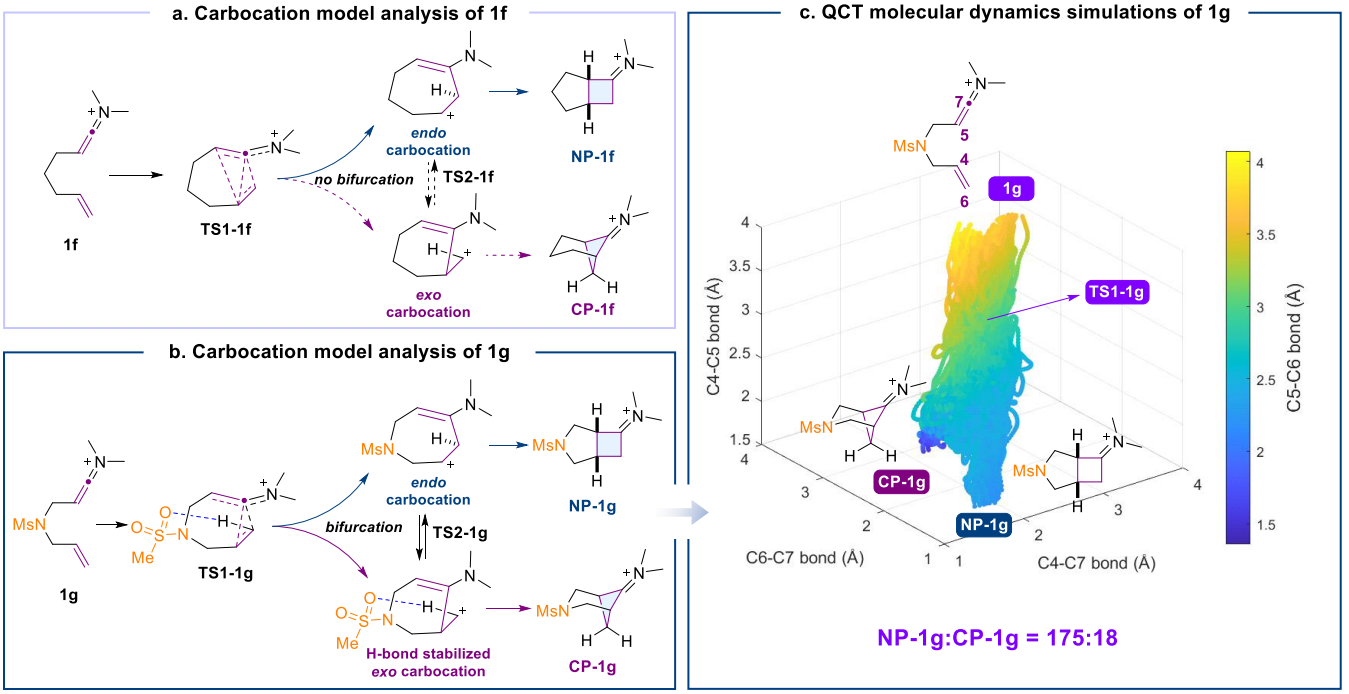

Figure 6. Carbocation model analysis of [2 + 2] cycloaddition of **1f** (a) and **1g** (b) and QCT molecular dynamics simulations (c) of [2 + 2] cycloaddition of **1g**.

https://doi.org/10.1021/jacs.3c00685
J. Am. Chem. Soc. 2023, 145, 9634−9645

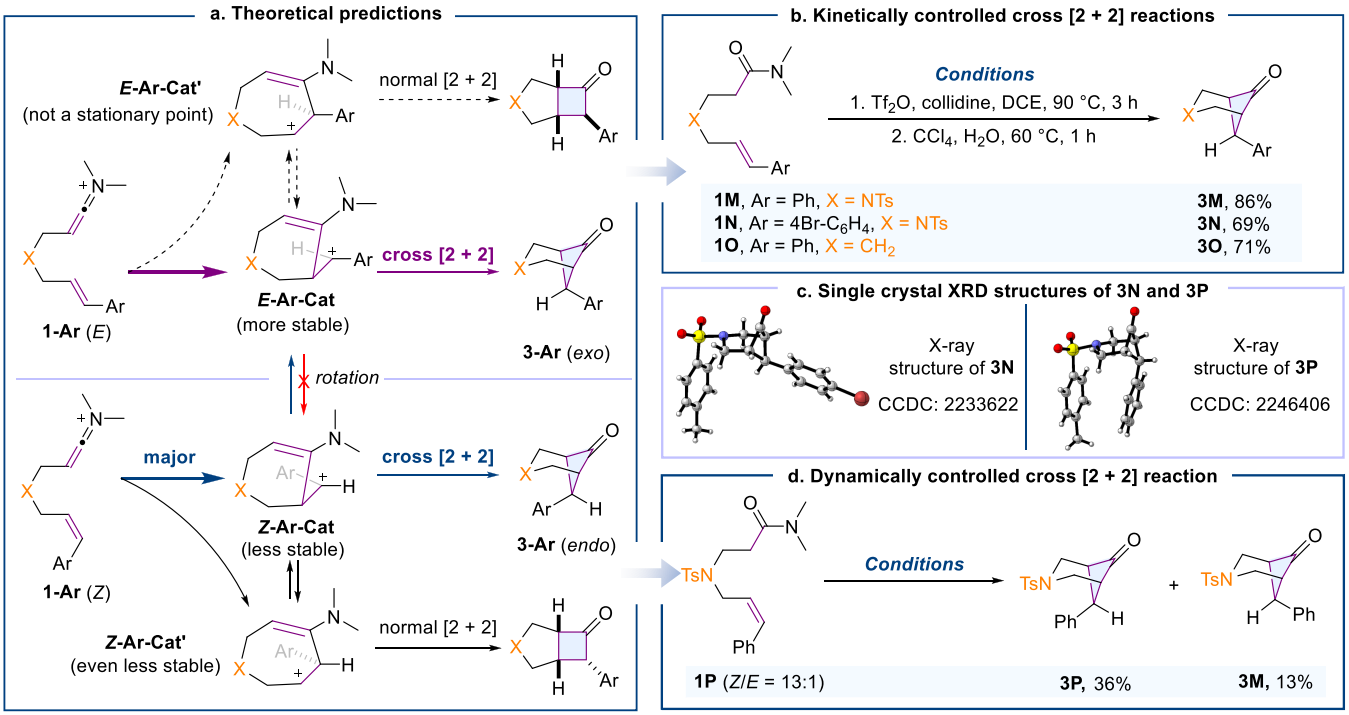

Figure 7. (a–d) More predictions and verifications of cross [2 + 2] cycloadditions. The yields given are average yields of isolated products for two runs. The reaction conditions in panel (d) are the same with those in panel (b).

substrate supported this prediction. We then predicted that substrates **1M**, **1N**, and **1O** (with a carbon tether), all with *E*-alkene, would give the same results (Figure 7b). We were happy to observe that these predictions were supported experimentally because all of them gave cross [2 + 2] products (Figure 7b,c).

We predicted that ene-keteniminium ions with *Z*-alkene could give dynamically controlled products (Figure 7a). Because the *exo* carbocation **Z-Ar-Cat** with repulsion between the tether and aryl group could have similar stabilities with *endo* carbocation **Z-Ar-Cat′** (**Z-Ar-Cat** is more stable than **Z-Ar-Cat′**). Computationally, we can locate an ambimodal transition state **TS1-1p** for ene-keteniminium ion **1p** (an analogue keteniminium ion of **1P**; see the SI). QCT molecular dynamics simulation (solution phase; see the SI) suggested that the minor normal [2 + 2] product could be observed because the *endo* carbocation is less stable by about 5 kcal/mol and most trajectories lead to cross products (77 trajectories to CP and 16 trajectories to NP in all 100 trajectories).

Experimentally (Figure 7d), we tested **1P** and found that no normal [2 + 2] product was observed. Cross [2 + 2] product **3P** (confirmed by X-ray analysis; Figure 7c) was obtained in 36% yield, together with its stereoisomer **3M**, which was formed by the rotation process of **Z-Ar-Cat** to **E-Ar-Cat**. Molecular dynamics simulations found that there is such a process leading to **E-Ar-Cat** (2 of 100 trajectories). Details are discussed in the SI. For **1-Ar** (*E*), the rotation process from **E-Ar-Cat** to **Z-Ar-Cat** could be much slower than the formation of the C–C bond (giving the stable cross [2 + 2] product), and consequently, only one product was obtained (Figure 7).

CONCLUSIONS

Based on *ab initio* quantum chemical calculations and molecular dynamics simulations, we found that the [2 + 2] cycloadditions of ene-keteniminium ions to give normal or cross [2 + 2] products have all three patterns of regiochemical control; namely, here, regiochemistry is controlled either kinetically, thermodynamically, or dynamically, affected by both substituents on the alkenes and tethers connecting the ene and keteniminium ion parts in substrates. For *α*-O-tethered substrates, a cyclopropane intermediate is formed first and the selectivity is determined by the subsequent rearrangement. These [2 + 2] reactions could be kinetically or thermodynamically controlled.

For *β*-N-tethered substrates, a carbocation model is proposed to explain the selectivity. If *endo* carbocation is more stable than *exo* carbocation, the normal [2 + 2] reaction can be favored kinetically over cross [2 + 2] cycloaddition. If *exo* carbocation is more stabilized than *endo* carbocation, the cross [2 + 2] reaction is favored over normal [2 + 2] reaction, either in a kinetically or dynamically controlled fashion, depending on the substituent (alkyl or aryl group) in the alkene part of the substrate (Scheme 3, Figures 5 and 7; more results of the reactions of ene-keteniminium ions with different combinations of substituents can be predicted by using these models). Our model also predicts that, the [2 + 2] reaction is dynamically controlled (both normal and cross [2 + 2] could be observed), if *endo* and *exo* carbocations have similar stabilities. These understandings guided us to design new experiments to achieve rarely observed cross [2 + 2] reactions, accessing products with challenging bicyclo[3.1.1]heptane skeletons. Also, new calculations and experiments have been applied to correct the misassigned [2 + 2] product. This study not only gives insightful mechanisms of the [2 + 2] reaction of ene-keteniminium ions but also implies that many competing reactions with carbocation intermediates could have similar patterns of regiochemical control.

https://doi.org/10.1021/jacs.3c00685
J. Am. Chem. Soc. 2023, 145, 9634–9645

COMPUTATIONAL METHODS

All the density functional theory calculations were carried out using Gaussian software.[16] Pruned integration grids with 99 radial shells and 590 angular points per shell were used. Geometry optimizations were performed at the ωB97X-D[17]/def2-SVP[18] level of theory in the gas phase.[19] The functional ωB97X-D was found to perform well in calculating organic reactions including keteniminium ions involved ones according to previous reports.[8c,20] Benchmarks of our system using CCSD(T)[21] as the reference were also done, and it was found that ωB97X-D indeed shows good performance (one of the best among the tested functionals; see the SI). Unscaled harmonic frequency calculations at the same level were performed to validate each structure as either a minimum or a transition state and to evaluate its zero-point energy and thermal corrections at 298.15 K. The SMD model[22] was used to evaluate the solvation effects. Intrinsic reaction coordinate (IRC)[23] calculations were used to confirm the transition states. Single-point energies were calculated at the DLPNO-CCSD(T)[24]/cc-pVTZ[25] (with the cc-pVTZ/C[26] auxiliary basis set, HF part accelerated with RIJK and cc-pVTZ/JK) level using the ORCA 4.2.1 software package.[27] "TightPNO" and "TightSCF" settings were applied during the single-point energy calculations. VTST including Wigner one-dimensional tunneling effect calculation of the free energy profile is based on generalized free energies of activation, which was obtained from KiSThelP.[28] 3D rendering molecular structures were produced by CYLview.[29] NCI analysis[30] was calculated by Multiwfn[31] and visualized by VMD.[32] All the discussed energy differences were based on Gibbs energies at 298.15 K (standard states are the hypothetical states at 1 mol/L), unless otherwise specified. To simplify the model, the NTs group was reduced to NMs and the pyrrolidine group was replaced by the dimethylamino group in calculations.

Molecular dynamics simulations were performed at the ωB97X-D/def2-SVP level of theory in the gas phase and the temperature was set to be 363.15 K, which is often used as the reaction temperature for ene-keteniminium salt intramolecular [2 + 2] cycloaddition experimentally. QCTs were initiated from the corresponding transition states and propagated forward and backward until either one of the products is formed (the forming C−C bond shorter than 1.6 Å) or the reactants are generated (all of the C4−C7, C4−C5, C6−C7, and C6−C5 bonds longer than 3.1 Å). The classical equations of motion were integrated with a velocity Verlet algorithm using Singleton's program Progdyn,[33] with the energies and derivatives computed on the fly with ωB97X-D/def2-SVP using Gaussian 09. The step length for integration was 1 fs. More details about the solution phase molecular dynamics can be found in the SI.

ASSOCIATED CONTENT

Supporting Information

The Supporting Information is available free of charge at https://pubs.acs.org/doi/10.1021/jacs.3c00685.

Experimental procedures, characterization data, NMR spectra, and computational details (PDF)

Accession Codes

CCDC 2233622 and 2246406 contain the supplementary crystallographic data for this paper. These data can be obtained free of charge via www.ccdc.cam.ac.uk/data_request/cif, or by emailing data_request@ccdc.cam.ac.uk, or by contacting The Cambridge Crystallographic Data Centre, 12 Union Road, Cambridge CB2 1EZ, UK; fax: +44 1223 336033.

AUTHOR INFORMATION

Corresponding Author

Zhi-Xiang Yu − *Beijing National Laboratory for Molecular Sciences (BNLMS), Key Laboratory of Bioorganic Chemistry and Molecular Engineering of Ministry of Education, College of Chemistry, Peking University, Beijing 100871, China;* orcid.org/0000-0003-0939-9727; Email: yuzx@pku.edu.cn

Author

Pan Zhang − *Beijing National Laboratory for Molecular Sciences (BNLMS), Key Laboratory of Bioorganic Chemistry and Molecular Engineering of Ministry of Education, College of Chemistry, Peking University, Beijing 100871, China*

Complete contact information is available at: https://pubs.acs.org/10.1021/jacs.3c00685

Notes

The authors declare no competing financial interest.

ACKNOWLEDGMENTS

This work was supported by the National Natural Science Foundation of China (21933003) and High-Performance Computing Platform of Peking University. We thank Dr. Yi Qiu at Peking University for X-ray single-crystal analysis. This paper is dedicated to Prof. K. N. Houk at UCLA on the occasion of his 80th birthday.

REFERENCES

(1) (a) Snider, B. B. Intramolecular Cycloaddition Reactions of Ketenes and Keteniminium Salts with Alkenes. *Chem. Rev.* **1988**, *88*, 793−811. (b) Markó, I.; Ronsmans, B.; Hesbain-Frisque, A.-M.; Dumas, S.; Ghosez, L. Intramolecular [2 + 2] Cycloadditions of Ketenes and Keteniminium Salts to Olefins. *J. Am. Chem. Soc.* **1985**, *107*, 2192−2194. (c) Snider, B. B.; Hui, R. A. H. F.; Kulkarni, Y. S. Intramolecular [2 + 2] Cycloadditions of Ketenes. *J. Am. Chem. Soc.* **1985**, *107*, 2194−2196. (d) Snider, B. B.; Hui, R. A. H. F. Intramolecular [2 + 2] Cycloadditions of Alkoxyketenes and Alkoxyketeniminium Salts. *J. Org. Chem.* **1985**, *50*, 5167−5176. (e) Snider, B. B.; Allentoff, A. J.; Walner, M. B. Intramolecular [2 + 2] cycloadditions of dialkylketenes with alkenes. Regiochemistry of intramolecular [2 + 2] cycloadditions of ketenes with alkenes. *Tetrahedron* **1990**, *46*, 8031−8042. (f) Brady, W. T.; Giang, Y. F. Intramolecular (2 + 2) cycloadditions of phenoxyketenes. *J. Org. Chem.* **1985**, *50*, 5177−5179. (g) Arya, F.; Bouquant, J.; Chuche, J. Preparation of 3-azabicyclo [3.2.0] heptenones by intramolecular [2 + 2] cycloaddition. *Tetrahedron Lett.* **1986**, *27*, 1913−1914.

(2) Fan, X.; Zhang, P.; Wang, Y.; Yu, Z.-X. Mechanism and Regioselectivity of Intramolecular [2 + 2] Cycloaddition of Ene−Ketenes: A DFT Study. *Eur. J. Org. Chem.* **2020**, 5985−5994.

(3) In ref 2, we named these carbocations as internal and external carbocations and one reviewer suggested us to use *endo* and *exo* carbocations. We thank this reviewer for this and adopt this new definition.

(4) For a review, see (a) Madelaine, C.; Valerio, V.; Maulide, N. Revisiting Keteniminium Salts: More than the Nitrogen Analogs of Ketenes. *Chem. − Asian J.* **2011**, *6*, 2224−2239. For example, see (b) Brady, W. T.; Giang, L.-S. F.; Weng, L.; Dad, M. M. Intramolecular [2 + 2] Cycloadditions of Ketene Iminium Salts to Carbon-Carbon Double Bonds. *J. Org. Chem.* **1987**, *52*, 2216−2220. (c) Gobeaux, B.; Ghosez, L. Intramolecular [2 + 2] Cycloadditions of Keteniminium Salts Derived from α- and β-Amino Acids. A Route to Azabicyclic Ketones. *Heterocycles* **1989**, *28*, 29−32. (d) Chen, L.-Y.; Ghosez, L. Study of Chiral Auxiliaries for the Intramolecular [2 + 2] Cycloaddition of a Keteniminium Salt to an Olefinic Double Bond. A New Asymmetric Synthesis of Cyclobutanones. *Tetrahedron Lett.* **1990**, *31*, 4467−4470. (e) Kolleth, A.; Lumbroso, A.; Tanriver, G.; Catak, S.; Sulzer-Mossé, S.; Mesmaeker, A. D. Synthesis of 4-membered ring alkaloid analogues via intramolecular [2 + 2] cycloaddition involving keteniminium salt intermediates. *Tetrahedron Lett.* **2017**, *58*, 2904−2909.

(5) For intermolecular cases, see (a) Ghosez, L. α-Chloroenamines: New Reagents for Organic Synthesis. *Angew. Chem., Int. Ed. Engl.*

1972, *11*, 852−853. (b) Marchand-Brynaert, J.; Ghosez, L. Cycloadditions of keteneimmonium cations to olefins and dienes. New synthesis of four-membered rings. *J. Am. Chem. Soc.* **1972**, *94*, 2870−2872. (c) Falmagne, J.-B.; Escudero, J.; Taleb-Sahraoui, S.; Ghosez, L. Cyclobutanone and Cyclobutenone Derivatives by Reaction of Tertiary Amides with Alkenes or Alkynes. *Angew. Chem., Int. Ed. Engl.* **1981**, *20*, 879−880. (d) Kolleth, A.; Lumbroso, A.; Tanriver, G.; Catak, S.; Sulzer-Mossé, S.; Mesmaeker, A. D. Synthesis of aminocyclobutanes via [2 + 2] cycloadditions involving keteniminium intermediates. *Tetrahedron Lett.* **2016**, *57*, 2697−2702.

(6) For a recent review, see (a) Subbaiah, M. A. M.; Meanwell, N. A. Bioisosteres of the Phenyl Ring: Recent Strategic Applications in Lead Optimization and Drug Design. *J. Med. Chem.* **2021**, *64*, 14046−14128. For recent examples, see (b) Li, B.-S.; Yang, B.-M.; Wang, S.-H.; Zhang, Y.-Q.; Cao, X.-P.; Tu, Y.-Q. Copper(I)-catalyzed intramolecular [2 + 2] cycloaddition of 1,6-enyne-derived ketenimine: an efficient construction of strained and bridged 7-substituted-3-heterobicyclo[3.1.1]heptan-6-one. *Chem. Sci.* **2012**, *3*, 1975−1979. (c) Frank, N.; Nugent, J.; Shire, B. R.; Pickford, H. D.; Rabe, P.; Sterling, A. J.; Zarganes-Tzitzikas, T.; Grimes, T.; Thompson, A. L.; Smith, R. C.; Schofield, C. J.; Brennan, P. E.; Duarte, F.; Anderson, E. A. Synthesis of meta-substituted arene bioisosteres from [3.1.1]-propellane. *Nature* **2022**, *611*, 721−726. (d) Zheng, Y.; Huang, W.; Dhungana, R. K.; Granados, A.; Keess, S.; Makvandi, M.; Molander, G. A. Photochemical Intermolecular [3σ + 2σ]-Cycloaddition for the Construction of Aminobicyclo[3.1.1]heptanes. *J. Am. Chem. Soc.* **2022**, *144*, 23685−23690.

(7) Maskeri, M. A.; Fernandes, A. J.; Mauro, G. D.; Maulide, N.; Houk, K. N. Taming Keteniminium Reactivity by Steering Reaction Pathways: Computational Predictions and Experimental Validations. *J. Am. Chem. Soc.* **2022**, *144*, 23358−23367.

(8) For some other keteniminium ions related mechanistic studies: (a) Saimoto, H.; Houge, C.; Hesbain-Frisque, A.-M.; Mockel, A.; Ghosez, L. Nonstereospecificity in the cycloadditions of keteneiminium salts to olefins. Evidence for a stepwise mechanism. *Tetrahedron Lett.* **1983**, *24*, 2251−2254. (b) Ding, W.-J.; Fang, D.-C. Theoretical Studies on Cycloaddition Reactions between Keteniminium Cations and Olefins. *J. Org. Chem.* **2001**, *66*, 6673−6678. (c) Ramirez, M.; Li, W.; Lam, Y.-H.; Ghosez, L.; Houk, K. N. Mechanisms and Conformational Control of (4 + 2) and (2 + 2) Cycloadditions of Dienes to Keteniminium Cations. *J. Org. Chem.* **2020**, *85*, 2597−2606. (d) Adam, J.-M.; Ghosez, L.; Houk, K. N. A Convergent Strategy for the Asymmetric Synthesis of Enantiomerically Pure Bicyclic Compounds by Using a Silicon-Directed Cycloaddition Reaction: The Synthesis of Enantiomerically Pure Bicyclo[3.2.0]-hept-2-en-6-one. *Angew. Chem., Int. Ed.* **1999**, *38*, 2728−2730. (e) Domingo, L. R.; Ríos-Gutiérrez, M.; Pérez, P. A DFT study of the ionic [2 + 2] cycloaddition reactions of keteniminium cations with terminal acetylenes. *Tetrahedron* **2015**, *71*, 2421−2427.

(9) Rehbein, J.; Carpenter, B. K. Do we fully understand what controls chemical selectivity? *Phys. Chem. Chem. Phys.* **2011**, *13*, 20906−20922.

(10) For selected reviews about reactions with dynamical effects, see (a) Ess, D. H.; Wheeler, S. E.; Iafe, R. G.; Xu, L.; Çelebi-Ölçüm, N.; Houk, K. N. Bifurcations on Potential Energy Surfaces of Organic Reactions. *Angew. Chem., Int. Ed.* **2008**, *47*, 7592−7601. (b) Hare, S. R.; Tantillo, D. J. Post-transition state bifurcations gain momentum − current state of the field. *Pure Appl. Chem.* **2017**, *89*, 679−698. (c) McLeod, D.; Thøgersen, M. K.; Jessen, N. I.; Jørgensen, K. A.; Jamieson, C. S.; Xue, X.-S.; Houk, K. N.; Liu, F.; Hoffmann, R. Expanding the Frontiers of Higher-Order Cycloadditions. *Acc. Chem. Res.* **2019**, *52*, 3488−3501.

(11) For selected examples about reactions with dynamic effects, see (a) Caramella, P.; Quadrelli, P.; Toma, L. An Unexpected Bispericyclic Transition Structure Leading to 4+2 and 2+4 Cycloadducts in the Endo Dimerization of Cyclopentadiene. *J. Am. Chem. Soc.* **2002**, *124*, 1130−1131. (b) Limanto, J.; Khuong, K. S.; Houk, K. N.; Snapper, M. L. An Unexpected Bispericyclic Transition Structure Leading to 4+2 and 2+4 Cycloadducts in the Endo Dimerization of Cyclopentadiene. *J. Am. Chem. Soc.* **2003**, *125*, 16310−16321. (c) Ussing, B. R.; Hang, C.; Singleton, D. A. Dynamic Effects on the Periselectivity, Rate, Isotope Effects, and Mechanism of Cycloadditions of Ketenes with Cyclopentadiene. *J. Am. Chem. Soc.* **2006**, *128*, 7594−7607. (d) Patel, A.; Chen, Z.; Yang, Z.; Gutierrez, O.; Liu, H.-w.; Houk, K. N.; Singleton, D. A. Dynamically Complex [6+4] and [4+2] Cycloadditions in the Biosynthesis of Spinosyn A. *J. Am. Chem. Soc.* **2016**, *138*, 3631−3634. (e) Xue, X.-S.; Jamieson, C. S.; Garcia-Borràs, M.; Dong, X.; Yang, Z.; Houk, K. N. Ambimodal Trispericyclic Transition State and Dynamic Control of Periselectivity. *J. Am. Chem. Soc.* **2019**, *141*, 1217−1221. (f) Jamieson, C. S.; Sengupta, A.; Houk, K. N. Cycloadditions of Cyclopentadiene and Cycloheptatriene with Tropones: All *Endo*-[6+4] Cycloadditions Are Ambimodal. *J. Am. Chem. Soc.* **2021**, *143*, 3918−3926. (g) Feng, Z.; Tantillo, D. J. Dynamic Effects on Migratory Aptitudes in Carbocation Reactions. *J. Am. Chem. Soc.* **2021**, *143*, 1088−1097. (h) Guo, W.; Hare, S. R.; Chen, S.-S.; Saunders, C. M.; Tantillo, D. J. C−H Insertion in Dirhodium Tetracarboxylate-Catalyzed Reactions despite Dynamical Tendencies toward Fragmentation: Implications for Reaction Efficiency and Catalyst Design. *J. Am. Chem. Soc.* **2022**, *144*, 17219−17231. (i) Yang, B.; Schouten, A.; Ess, D. H. Direct Dynamics Trajectories Reveal Nonstatistical Coordination Intermediates and Demonstrate that σ and π-Coordination Are Not Required for Rhenium(I)-Mediated Ethylene C−H Activation. *J. Am. Chem. Soc.* **2021**, *143*, 8367−8374. (j) Carlsen, R.; Wohlgemuth, N.; Carlson, L.; Ess, D. H. Dynamical Mechanism May Avoid High-Oxidation State Ir(V)−H Intermediate and Coordination Complex in Alkane and Arene C−H Activation by Cationic Ir(III) Phosphine. *J. Am. Chem. Soc.* **2018**, *140*, 11039−11045. (k) Lee, S.; Goodman, J. M. Rapid Route-Finding for Bifurcating Organic Reactions. *J. Am. Chem. Soc.* **2020**, *142*, 9210−9219. (l) Zhang, L.; Wang, Y.; Yao, Z.-J.; Wang, S.; Yu, Z.-X. Kinetic or Dynamic Control on a Bifurcating Potential Energy Surface? An Experimental and DFT Study of Gold-Catalyzed Ring Expansion and Spirocyclization of 2-Propargyl-β-tetrahydrocarbolines. *J. Am. Chem. Soc.* **2015**, *137*, 13290−13300.

(12) There is a stepwise isomerization pathway from **NP-1e** to **CP-1e**, which is 0.2 kcal/mol more favored over the concerted pathway (see the SI for details).

(13) This is an empirical time criterion, which is five times as long as the time criterion for a dynamically stepwise process (larger than 60 fs) defined by Houk et al., because there are real intermediates to pass through in our trajectories. For Houk's definition, see (a) Black, K.; Liu, P.; Xu, L.; Doubleday, C.; Houk, K. N. Dynamics, transition states, and timing of bond formation in Diels-Alder reactions. *Proc. Natl. Acad. Sci. U. S. A.* **2012**, *109*, 12860−12865. (b) Yang, Z.; Jamieson, C. S.; Xue, X.-S.; Garcia-Borràs, M.; Benton, T.; Dong, X.; Liu, F.; Houk, K. N. Mechanisms and Dynamics of Reactions Involving Entropic Intermediates. *Trends in Chemistry* **2019**, *1*, 22−34.

(14) (a) Doubleday, C.; Camp, R. N.; King, H. F.; McIver, J. W.; Mullally, D.; Page, M. Is Tetramethylene an Intermediate? *J. Am. Chem. Soc.* **1984**, *106*, 447−448. (b) Gonzalez-James, O. M.; Kwan, E. E.; Singleton, D. A. Entropic Intermediates and Hidden Rate-Limiting Steps in Seemingly Concerted Cycloadditions. Observation, Prediction, and Origin of an Isotope Effect on Recrossing. *J. Am. Chem. Soc.* **2012**, *134*, 1914−1917.

(15) Truhlar, D. G.; Garrett, B. C. Variational transition-state theory. *Acc. Chem. Res.* **1980**, *13*, 440−448.

(16) Frisch, M. J.; Trucks, G. W.; Schlegel, H. B.; Scuseria, G. E.; Robb, M. A.; Cheeseman, J. R.; Scalmani, G.; Barone, V.; Mennucci, B.; Petersson, G. A.; Nakatsuji, H.; Caricato, M.; Li, X.; Hratchian, H. P.; Izmaylov, A. F.; Bloino, J.; Zheng, G.; Sonnenberg, J. L.; Hada, M.; Ehara, M.; Toyota, K.; Fukuda, R.; Hasegawa, J.; Ishida, M.; Nakajima, T.; Honda, Y.; Kitao, O.; Nakai, H.; Vreven, T.; Montgomery, J. A., Jr.; Peralta, J. E.; Ogliaro, F.; Bearpark, M.; Heyd, J. J.; Brothers, E.; Kudin, K. N.; Staroverov, V. N.; Keith, T.; Kobayashi, R.; Normand, J.; Raghavachari, K.; Rendell, A.; Burant, J. C.; Iyengar, S. S.; Tomasi, J.; Cossi, M.; Rega, N.; Millam, J. M.; Klene, M.; Knox, J. E.; Cross, J. B.; Bakken, V.; Adamo, C.; Jaramillo,

https://doi.org/10.1021/jacs.3c00685
J. Am. Chem. Soc. 2023, 145, 9634−9645

J.; Gomperts, R.; Stratmann, R. E.; Yazyev, O.; Austin, A. J.; Cammi, R.; Pomelli, C.; Ochterski, J. W.; Martin, R. L.; Morokuma, K.; Zakrzewski, V. G.; Voth, G. A.; Salvador, P.; Dannenberg, J. J.; Dapprich, S.; Daniels, A. D.; Farkas, Ö.; Foresman, J. B.; Ortiz, J. V.; Cioslowski, J.; Fox, D. J. *Gaussian 09, Revision E.01*; Gaussian, Inc.: Wallingford, CT, 2013.

(17) Chai, J.-D.; Head-Gordon, M. Long-range corrected hybrid density functionals with damped atom-atom dispersion corrections. *Phys. Chem. Chem. Phys.* **2008**, *10*, 6615−6620.

(18) Weigend, F.; Ahlrichs, R. Balanced basis sets of split valence, triple zeta valence and quadruple zeta valence quality for H to Rn: Design and assessment of accuracy. *Phys. Chem. Chem. Phys.* **2005**, *7*, 3297−3305.

(19) To obtain the intrinsic selectivities and reduce computational cost, we performed the structure optimization and molecular dynamics in the gas phase. Considering that the reactions were run in DCE, we also carried out structure optimization and molecular dynamics in solution for representative cases, finding that there is no distinct difference between these simulations (see the SI for details).

(20) (a) Zhao, Y.; Truhlar, D. G. Density Functional Theory for Reaction Energies: Test of Meta and Hybrid Meta Functionals, Range-Separated Functionals, and Other High-Performance Functionals. *J. Chem. Theory Comput.* **2011**, *7*, 669−676. (b) Barber, J. S.; Yamano, M. M.; Ramirez, M.; Darzi, E. R.; Knapp, R. R.; Liu, F.; Houk, K. N.; Garg, N. K. Diels−Alder Cycloadditions of Strained Azacyclic Allenes. *Nat. Chem.* **2018**, *10*, 953−960.

(21) Purvis, G. D., III; Bartlett, R. J. A Full Coupled-Cluster Singles and Doubles Model: The Inclusion of Disconnected Triples. *J. Chem. Phys.* **1982**, *76*, 1910−1918.

(22) Marenich, A. V.; Cramer, C. J.; Truhlar, D. G. Universal Solvation Model Based on Solute Electron Density and on a Continuum Model of the Solvent Defined by the Bulk Dielectric Constant and Atomic Surface Tensions. *J. Phys. Chem. B* **2009**, *113*, 6378−6396.

(23) Fukui, K. The path of chemical reactions - the IRC approach. *Acc. Chem. Res.* **1981**, *14*, 363−368.

(24) (a) Riplinger, C.; Neese, F. An Efficient and Near Linear Scaling Pair Natural Orbital Based Local Coupled Cluster Method. *J. Chem. Phys.* **2013**, *138*, No. 034106. (b) Riplinger, C.; Sandhoefer, B.; Hansen, A.; Neese, F. Natural Triple Excitations in Local Coupled Cluster Calculations with Pair Natural Orbitals. *J. Chem. Phys.* **2013**, *139*, 134101. (c) Neese, F.; Atanasov, M.; Bistoni, G.; Maganas, D.; Ye, S. Chemistry and Quantum Mechanics in 2019: Give Us Insight *and* Numbers. *J. Am. Chem. Soc.* **2019**, *141*, 2814−2824.

(25) (a) Dunning, T. H., Jr. Gaussian basis sets for use in correlated molecular calculations. I. The atoms boron through neon and hydrogen. *J. Chem. Phys.* **1989**, *90*, 1007−1023. (b) Woon, D. E.; Dunning, T. H., Jr. Gaussian basis sets for use in correlated molecular calculations. III. The atoms aluminum through argon. *J. Chem. Phys.* **1993**, *98*, 1358−1371.

(26) Weigend, F.; Köhn, A.; Hättig, C. Efficient use of the correlation consistent basis sets in resolution of the identity MP2 calculations. *J. Chem. Phys.* **2002**, *116*, 3175−3183.

(27) (a) Neese, F. The ORCA Program System. *Wiley Interdiscip. Rev.: Comput. Mol. Sci.* **2012**, *2*, 73−78. (b) Neese, F. Software Update: The ORCA Program System, Version 4.0. *Wiley Interdiscip. Rev.: Comput. Mol. Sci.* **2017**, *8*, No. e1327.

(28) Canneaux, S.; Bohr, F.; Henon, E. KiSThelP: A program to predict thermodynamic properties and rate constants from quantum chemistry results. *J. Comput. Chem.* **2014**, *35*, 82−93.

(29) Legault, C. Y. *CYLview20*; Université de Sherbrooke, 2020; http://www.cylview.org (accessed 24 January, 2021).

(30) Johnson, E. R.; Keinan, S.; Mori-Sánchez, P.; Contreras-García, J.; Cohen, A. J.; Yang, W. Revealing Noncovalent Interactions. *J. Am. Chem. Soc.* **2010**, *132*, 6498−6506.

(31) Lu, T.; Chen, F. Multiwfn: A Multifunctional Wavefunction Analyzer. *J. Comput. Chem.* **2012**, *33*, 580−592.

(32) Humphrey, W.; Dalke, A.; Schulten, K. V. M. D. Visual molecular dynamics. *J. Mol. Graphics* **1996**, *14*, 33−38.

(33) (a) Singleton, D. A.; Wang, Z. H. Isotope Effects and the Nature of Enantioselectivity in the Shi Epoxidation. The Importance of Asynchronicity. *J. Am. Chem. Soc.* **2005**, *127*, 6679−6685. (b) Biswas, B.; Collins, S. C.; Singleton, D. A. Dynamics and a Unified Understanding of Competitive [2,3]- and [1,2]-Sigmatropic Rearrangements Based on a Study of Ammonium Ylides. *J. Am. Chem. Soc.* **2014**, *136*, 3740−3743. (c) Plata, R. E.; Singleton, D. A. Controlling Selectivity by Controlling the Path of Trajectories. *J. Am. Chem. Soc.* **2015**, *137*, 14244−14247.

https://doi.org/10.1021/jacs.3c00685
J. Am. Chem. Soc. 2023, 145, 9634−9645